JOURNAL OF GEOPHYSICAL RESEARCH, VOL. 110, B12105, doi:10.1029/2004JB003463, 2005

Correction of seafloor magnetotelluric data for topographic effects during inversion

Kiyoshi Baba[1]
Institute for Research on Earth Evolution, Japan Agency for Marine-Earth Science and Technology, Yokosuka, Japan

Alan D. Chave
Department of Applied Ocean Physics and Engineering, Woods Hole Oceanographic Institution, Woods Hole, Massachusetts, USA

Received 1 October 2004; revised 11 July 2005; accepted 22 August 2005; published 14 December 2005.

[1] The large contrast in electrical conductivity between seawater and the underlying seafloor accumulates boundary electric charges which can severely distort observed electric and magnetic fields. For marine magnetotelluric (MT) studies, correcting this topographic effect is critical to obtaining accurate conductivity models for the mantle. Previously, correction for topography was based on the thin sheet approximation which breaks down at periods under ~1000 s in the deep ocean. This paper introduces an analysis method for seafloor MT data which combines removal of three-dimensional (3-D) topographic effects with inversion of the data for 2-D structure. The observed MT impedance is first corrected to a flat-lying seafloor datum using the observed bathymetry without invoking the thin sheet approximation. The corrected MT response is then inverted in a flat seafloor model space. Because of coupling between topographic effects and deeper structure, the correction and inversion steps are iterated until changes in each become small. The procedure is verified using synthetic and real data. Tests for synthetic 3-D topography over a half-space show that the method closely recovers the true half-space model after a few iterations. The procedure is also applied to real data collected in the Mantle Electromagnetic and Tomography (MELT) experiment on the East Pacific Rise at 17°S.

Citation: Baba, K., and A. D. Chave (2005), Correction of seafloor magnetotelluric data for topographic effects during inversion, *J. Geophys. Res.*, *110*, B12105, doi:10.1029/2004JB003463.

1. Introduction

[2] Marine magnetotelluric (MT) studies have proliferated since the late 1970s, and are elucidating the electrical conductivity structure of Earth's mantle in diverse tectonic settings, including normal ocean basins, marginal basins, subduction systems, hot spots, and mid-ocean ridges [e.g., *Filloux*, 1977; *Oldenburg et al.*, 1984; *Wannamaker et al.*, 1989; *Nolasco et al.*, 1998; *Evans et al.*, 1999; N. Seama et al., 1-D electrical conductivity structure beneath the Philippine Sea: Results from an ocean bottom magnetotelluric survey, submittted to *Physics of the Earth and Planetary Interiors*, 2005]. As data quality and density improve, interest has been focused on more accurate and reliable determination of earth structure in increasingly complex terranes. Enhanced correction for the strong effect of seafloor topography on the MT response is key to this transition.

[3] Distortion of the electromagnetic field due to near surface conductivity heterogeneities (including topography) and its treatment in data analysis are long-standing problems in electromagnetic geophysics [e.g., *Berdichevsky et al.*, 1989; *Jiracek*, 1990]. Distorted fields typically present significant problems during geophysical inversion, as it is difficult to simultaneously resolve the small-scale (relative to the induction scale) heterogeneity that produces distortion and yet include the much larger-scale, heterogeneous structure of the underlying mantle which is of geophysical interest. For this reason, the use of direct three-dimensional (3-D) inversion methods that include topography is unfeasible. Moreover, mantle structure is frequently approximately 1-D or 2-D in many tectonic settings even if the topography is 3-D, and so a direct inversion approach is not efficient.

[4] The now standard approach to this problem is application of a tensor decomposition model [e.g., *Bahr*, 1988; *Groom and Bailey*, 1989; *Chave and Smith*, 1994; *Utada and Munekane*, 2000] to the observed MT response to remove galvanic distortion and recover the regional response. However, such methods fail to give a statistically significant fit to many seafloor data sets even when magnetic field galvanic distortion (which is typically large [*White et al.*, 1997]) is included, in part owing to a breakdown of the tensor decomposition model assumptions.

[1]Now at Earthquake Research Institute, University of Tokyo, Tokyo, Japan.

0148-0227/05/2004JB003463$09.00

In particular, it is unlikely that the regional electric field remains uniform across large seafloor topographic heterogeneities or that the electric field at the heterogeneity can be approximated by its value at the observation point, both of which are implicit to any tensor decomposition method [*Chave and Smith*, 1994]. In addition, self-induction is frequently important for seafloor topographic distortion, but is not accommodated in current tensor decomposition models.

[5] A reasonable alternative is a two stage approach in which topographic effects are first stripped from the observed MT response and the corrected response is then inverted in a model space of suitable dimension but without topographic variation. *Heinson and Lilley* [1993] introduced such a correction method using the 3-D thin sheet approximation [*Vasseur and Weidelt*, 1977] for topography over a 1-D mantle model in Tasman Sea data. *Nolasco et al.* [1998] also used a 3-D thin sheet model over a 1-D mantle to estimate electric and magnetic distortion from islands and bathymetry, and removed it from Society Islands seafloor MT data prior to 2-D mantle inversion. *Koyama* [2002] devised an iterative correction method for the land-ocean boundary effect in basin-scale integral equation modeling of the Pacific region. All of these algorithms implicitly assume a mantle conductivity structure during simulation of topographic effects, and hence mutual coupling must be checked to assure consistency. *Heinson and Lilley* [1993] and *Nolasco et al.* [1998] estimated the topographic effect by trial and error forward modeling, and then inverted the corrected data. *Koyama* [2002] iterated between the correction and inversion of the corrected data, which requires only an initial guess for mantle structure, and hence is more objective.

[6] The critical component of all two stage approaches lies in the forward modeling method that must accurately simulate the topographic effect. Previous work used the thin sheet approximation to model 3-D fluctuations in ocean depth as variations in conductance. However, the inhomogeneous thin sheet approximation is both difficult to apply over a 2-D or 3-D mantle model and increasingly inaccurate at periods under about 1000 s in the deep ocean, as the electromagnetic skin depth becomes comparable to the water depth. Yet, many critical processes of geophysical interest, such as melt transport beneath mid-ocean ridges, are inherently 2-D/3-D and best resolved at periods at or below this value.

[7] *Baba and Seama* [2002] recently introduced a modeling technique called FS3D which can incorporate precise 3-D topography over arbitrary subsurface structure without invoking the thin sheet approximation. The FS3D method converts seafloor topography to 3-D changes in the electrical conductivity and magnetic permeability of blocks bounding a flat-lying seafloor, resulting in considerable simplification compared to a full 3-D simulation. Direct inversion based on FS3D is not efficient because the fine horizontal meshing needed to simulate topography is not necessary to model large-scale heterogeneities in the mantle.

[8] In this paper, we propose a topographic effect correction and mantle structure inversion algorithm for seafloor MT data which is an improvement on previous methods. Forward modeling to remove topographic effects using FS3D corrects the observed MT responses to a flat-lying datum. The corrected data are then inverted using standard algorithms, and the resulting structure is used to recorrect the observations until convergence is achieved.

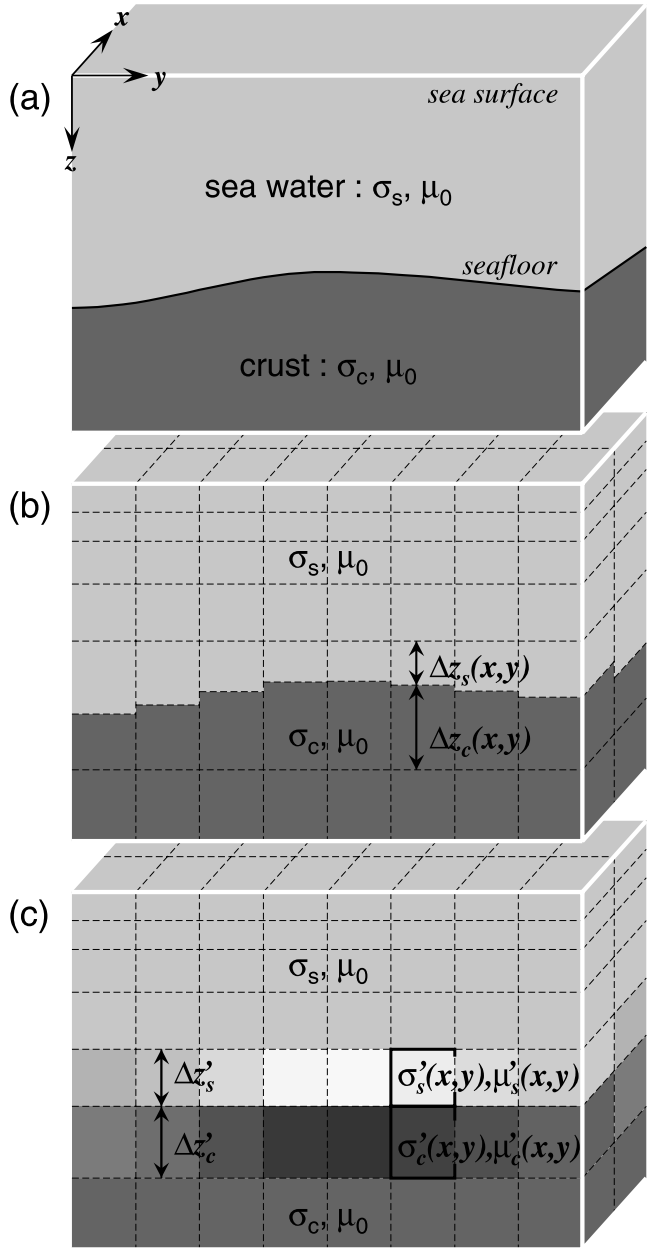

Figure 1. Cartoon illustrating the principle of FS3D: (a) the real Earth, (b) Earth divided into rectangular blocks, so that topographic change is expressed by variations in the thickness of the blocks at the two layers bounding the seafloor, and (c) the FS3D model where the seafloor is flattened and the conductivity and permeability in the two layers are converted to tensors as conductance and permeance in each direction are conserved. After *Baba and Seama* [2002] with permission from Blackwell Publishing.

[9] In section 2, the principle of the FS3D algorithm is introduced along with an overview of the topographic correction method. In section 3, the method is tested on synthetic 3-D topography over a half-space, and in section 4 its utility is demonstrated on real data collected during the

Mantle ELectromagnetic and Tomography experiment on the East Pacific Rise at 17°S [*Evans et al.*, 1999]. Finally, in section 5, a physical interpretation of topographic correction methods and the results of some accuracy tests are discussed.

2. The Method

[10] The method proposed in this paper is based on iteration between two stages as previously suggested by *Koyama* [2002]; the first stage is topographic stripping of the observed MT responses and the second stage is inversion of the stripped responses for mantle structure. In the initial, correction phase, the MT response of a subsurface model with and without 3-D topography is numerically simulated, and the topographic effect is estimated. The topographic effect is then removed from the observed MT response. In the second phase, the corrected MT response is inverted for structure using any suitable method at the appropriate mantle dimensionality. The model space for the inversion contains no topography since the MT responses are corrected to a flat-lying datum. The topographic stripping phase requires an assumed subsurface structure, and hence the topographic correction is in principle dependent on the resulting model. This nonlinear dependence may be treated iteratively; the correction phase is carried out again using the subsurface structure obtained from the inversion phase at the previous iteration until neither the topographic correction nor the mantle model change significantly. The final result is typically insensitive to the initial subsurface model. The simplest and most objective initial choice is a half-space model, although more complicated situations may easily be accommodated.

[11] Simulation of the MT response to subsurface structure in the presence of 3-D topography is achieved using *Baba and Seama*'s [2002] FS3D method. This plays a key role in the iterative procedure because it enables precise yet efficient modeling of topographic effects with an arbitrary subsurface structure. The principle of the FS3D method is conversion of a change in topography into a change in anisotropic conductivity and permeability at the boundary (Figure 1). The conversion is applied in two layers of a discretized earth model which bound the seafloor

$$\boldsymbol{\sigma}'_s = \begin{bmatrix} \frac{\Delta z_s}{\Delta z'_s}\sigma_s & 0 & 0 \\ 0 & \frac{\Delta z_s}{\Delta z'_s}\sigma_s & 0 \\ 0 & 0 & \frac{\Delta z'_s}{\Delta z_s}\sigma_s \end{bmatrix}, \tag{1}$$

$$\boldsymbol{\sigma}'_c = \begin{bmatrix} \frac{\Delta z_c}{\Delta z'_c}\sigma_c & 0 & 0 \\ 0 & \frac{\Delta z_c}{\Delta z'_c}\sigma_c & 0 \\ 0 & 0 & \frac{\Delta z'_c}{\Delta z_c}\sigma_c \end{bmatrix}, \tag{2}$$

$$\boldsymbol{\mu}'_s = \begin{bmatrix} \frac{\Delta z_s}{\Delta z'_s}\mu_0 & 0 & 0 \\ 0 & \frac{\Delta z_s}{\Delta z'_s}\mu_0 & 0 \\ 0 & 0 & \frac{\Delta z'_s}{\Delta z_s}\mu_0 \end{bmatrix}, \tag{3}$$

$$\boldsymbol{\mu}'_c = \begin{bmatrix} \frac{\Delta z_c}{\Delta z'_c}\mu_0 & 0 & 0 \\ 0 & \frac{\Delta z_c}{\Delta z'_c}\mu_0 & 0 \\ 0 & 0 & \frac{\Delta z'_c}{\Delta z_c}\mu_0 \end{bmatrix}, \tag{4}$$

where in a Cartesian coordinate system (x, y, z), Δz_s and Δz_c are the thickness of water or crust within the respective layer (hereafter subscripts s and c denote seawater and crust, respectively), while σ_s and σ_c are the corresponding electrical conductivities and μ_s and μ_c are the corresponding magnetic permeabilities (μ_0 is the value for free space). The prime denotes the value after conversion. $\Delta z_s(x, y)$ and $\Delta z_c(x, y)$, which are functions of horizontal position because of 3-D topography, are transformed to a homogeneous $\Delta z'_s$ and $\Delta z'_c$ which are equivalent to the vertical mesh size of the bounding layers so that the seafloor is flattened. Through the conversion, conductance and permeance are conserved in the x, y, and z directions; they are proportional to a section perpendicular to the direction of the gridded blocks and inversely proportional to the distance parallel to the direction of the blocks. As a result, the conductivity and permeability are anisotropic and may have different values in each spatial direction in the blocks bounding the seafloor. The electric and magnetic fields (**E** and **H**), current density (**J**), and magnetic induction (**B**) for the two layers are also converted as follows (with the subscripts s and c omitted)

$$\mathbf{E}' = \left[E_x, E_y, \frac{\Delta z}{\Delta z'}E_z\right]^T, \tag{5}$$

$$\mathbf{H}' = \left[H_x, H_y, \frac{\Delta z}{\Delta z'}H_z\right]^T, \tag{6}$$

$$\mathbf{J}' = \left[\frac{\Delta z}{\Delta z'}J_x, \frac{\Delta z}{\Delta z'}J_y, J_z\right]^T, \tag{7}$$

$$\mathbf{B}' = \left[\frac{\Delta z}{\Delta z'}B_x, \frac{\Delta z}{\Delta z'}B_y, B_z\right]^T. \tag{8}$$

[12] Solving the Maxwell equations for the flattened $\mathbf{E}'$, $\mathbf{H}'$, $\mathbf{J}'$, $\mathbf{B}'$, $\boldsymbol{\sigma}'$, and $\boldsymbol{\mu}'$ is mathematically identical to solving the equations for the original **E**, **H**, **J**, **B**, σ, and μ_0. The numerical method used for the FS3D modeling is based on *Mackie et al.*'s [1994] 3-D modeling algorithm. Second-order equations in $\mathbf{H}'$ are derived based on a staggered grid finite difference approximation and solved by the same relaxation scheme as *Mackie et al.* [1994] used, except for

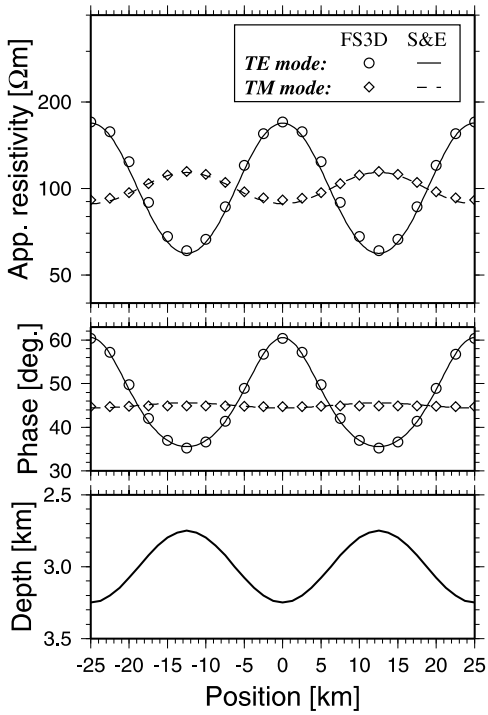

Figure 2. Comparison of 2-D topographic responses calculated analytically [*Schwalenberg and Edwards*, 2004] and using FS3D. Lines and symbols are the analytic and FS3D responses for the TE and TM modes, respectively. The parameters of the 2-D sinusoidal bathymetry model (see text) are $\lambda = 25$ km and $\Delta = 0.25$ km so that the maximum slope is about 3.6°. The period is 1000 s.

a divergence of **H** correction to improve the convergence properties of the relaxation solution. Instead, FS3D corrects the $\mathbf{H}'$ field to eliminate the divergence of $\mathbf{B}' = \boldsymbol{\mu}'\mathbf{H}'$ because $\boldsymbol{\mu}'$ may change between the two layers bounding the seafloor.

[13] The accuracy of FS3D is briefly demonstrated through a comparison with analytical solutions. *Schwalenberg and Edwards* [2004] presented analytical solutions for the MT response in the presence of 2-D sinusoidal topography. The bathymetric variation is given by $z = \Delta \cos(2\pi y/\lambda)$, where y and z are the horizontal and vertical positions, respectively. Figure 2 compares the analytical and FS3D responses to bathymetry for $\Delta = 0.25$ km, $\lambda = 25$ km, and with conductivities of 3.2 and 0.01 S m^{-1}, respectively, for seawater and the underlying medium. The two responses are in good agreement. The difference in response for the two methods for various wavelengths and periods were investigated to determine the range over which the FS3D method is accurate. Table 1 shows the root-mean-square (RMS) relative difference of the apparent resistivity and the RMS absolute difference of phase as a function of position. The FS3D and analytic solutions generally agree within 5% in apparent resistivity and 1 degree in phase, but the discrepancy becomes somewhat larger as the slope increases. However, seafloor topography measured from shipboard soundings display slopes of at most 5 degrees on horizontal scales of order the water depth (see Figure 10 in section 4). Therefore the FS3D method is accurate enough to model seafloor topography at measurable scales.

[14] With FS3D, a comparatively coarse grid with anisotropic conductivity and permeability across the seafloor substitute for much finer vertical meshing to adequately resolve topography in a full 3-D simulation. Numerical experiments demonstrate that the reduction in computational burden from introducing larger, more regular grid cells far outweighs the added complexity arising from incorporating the simple triaxial tensors in (1)–(4). Moreover, arbitrary, 2-D or 3-D, subsurface structure can be treated because FS3D is a fully 3-D modeling method that can be incorporated into 2-D or 3-D simulations, while only a subsurface 1-D structure is feasible for thin sheet modeling. This enables iteration of a realistic topographic correction in the presence of complex mantle structure obtained during the inversion step.

[15] Correction of the MT impedance tensor is achieved by assuming a theoretical relationship

$$\mathbf{Z} = \mathbf{Z}_t\mathbf{Z}_m, \tag{9}$$

where $\mathbf{Z}$ is the MT response which includes the influence of topography, $\mathbf{Z}_t$ is a tensor describing the topographic effect, and $\mathbf{Z}_m$ is the response to mantle structure without topography. This relationship was introduced by *Heinson and Lilley* [1993], although the approximation that $\mathbf{Z}_m$ is 1-D was also applied. In this study, all elements in (9) are complex 2×2 tensors and $\mathbf{Z}_m$ may be the response to a 2-D or 3-D mantle, and hence the method can be applied in any tectonic setting. Note that this multiplicative relation is similar to that for galvanic decomposition except that $\mathbf{Z}_t$ becomes real rather than complex, and ultimately flows from an integral equation description of electromagnetic distortion, as derived by *Groom and Bahr* [1992] and *Chave and Smith* [1994]. $\mathbf{Z}_t$ can be estimated from forward

Table 1. RMS Relative Difference for Apparent Resistivity and the RMS Absolute Difference for Phase Between the FS3D and Analytical Solutions as a Function of Horizontal Position[a]

	λ, km (Maximum Gradient, deg)		
Periods, s	10 (8.9)	25 (3.6)	50 (1.8)
	ϕ_{TE}		
316.23	2.7	0.7	1.1
1000.0	1.5	0.4	1.7
3162.3	0.9	0.3	0.5
	ϕ_{TM}		
316.23	0.7	0.9	1.3
1000.0	1.4	0.8	0.7
3162.3	1.7	0.6	0.3
	ρ_{TE}		
316.23	12.1	7.0	17.9
1000.0	8.1	4.0	5.4
3162.3	5.4	3.2	2.8
	ρ_{TM}		
316.23	9.6	2.3	1.5
1000.0	10.0	1.6	2.6
3162.3	12.9	1.4	3.4

[a]Apparent resistivity is in % and RMS absolute difference for phase is in degrees.

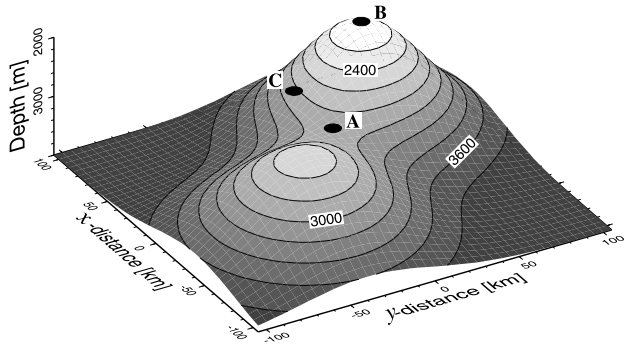

Figure 3. A synthetic seafloor topography model at a contour interval of 200 m. The solid circles with labels are the positions where synthetic MT responses are calculated. See text for details.

modeling of $\mathbf{Z}$ and $\mathbf{Z}_m$ using the FS3D method. The mantle structure must be provided a priori in the initial stage of solution. Once $\mathbf{Z}_t$ is obtained, we can correct the observed MT response, $\mathbf{Z}_o$. Applying (9) to $\mathbf{Z}_o$ and rearranging yields

$$\mathbf{Z}_c = \mathbf{Z}_t^{-1}\mathbf{Z}_o, \tag{10}$$

where $\mathbf{Z}_c$ is the response corrected for topographic effects that corresponds to the theoretical entity $\mathbf{Z}_m$. In practice, we can calculate $\mathbf{Z}_c$ from the observed MT response ($\mathbf{Z}_o$) and the modeled responses ($\mathbf{Z}$ and $\mathbf{Z}_m$) while skipping the calculation of $\mathbf{Z}_t$ to give

$$\mathbf{Z}_c = \mathbf{Z}_t^{-1}\mathbf{Z}_o = \left(\mathbf{Z}\mathbf{Z}_m^{-1}\right)^{-1}\mathbf{Z}_o = \mathbf{Z}_m\mathbf{Z}^{-1}\mathbf{Z}_o. \tag{11}$$

$\mathbf{Z}_c$ is then inverted in a model space with a flat seafloor. In the subsequent stages of the solution, the model obtained from inversion of $\mathbf{Z}_c$ is used to recorrect $\mathbf{Z}_o$. The iterative solution terminates under any suitable criterion. We have adopted the RMS misfit between $\mathbf{Z}$ and $\mathbf{Z}_o$ in the domain of log apparent resistivity, log ρ, and phase, ϕ,

$$\mathrm{RMS} = \sqrt{\frac{1}{2N}\sum_{i=1}^{N}\left\{\left[\frac{\log(\rho_{oi}/\rho_i)}{\delta\log\rho_{oi}}\right]^2 + \left[\frac{\phi_{oi}-\phi_i}{\delta\phi_{oi}}\right]^2\right\}}, \tag{12}$$

where δ log ρ_o and $\delta\phi_o$ are the estimated errors in log apparent resistivity and phase, and N is the number of data. If the RMS misfit change is below a threshold value (typically 1–2%), the solution is terminated.

3. Synthetic Data Example

[16] The method is first tested using synthetic data for simple 3-D topography over a 1-D mantle. The topography model contains two seamounts whose depth varies between 2000 and 4000 m (Figure 3). The horizontal model space extends over 1000 km from the center and hence well beyond the edge of the topography. The topography model is discretized every 10 km in the horizontal and used to flatten the seafloor to 3000 m water depth, converting topography into an equivalent lateral change in the electrical conductivity and magnetic permeability in the two layers bounding the seafloor. A 100 Ω m half-space is taken as the subsurface resistivity. The electromagnetic field on the flattened seafloor is simulated by FS3D for 11 periods equally spaced on a log scale between 10^2 and 10^5 seconds. The MT response is then calculated from the horizontal electromagnetic field.

[17] We first demonstrate the magnitude of the topographic effect on the MT response at three positions: Site A is at the saddle between the two seamounts, site B is at the summit of the larger seamount, and site C is on the flank of the larger seamount. The calculated apparent resistivities and phases are plotted in Figure 4. Since the assumed mantle structure is a 100 Ω m half-space, the response in the absence of topography is a constant 100 Ω m apparent resistivity and a 45 or -135 degree phase in the off-diagonal terms, and a zero response in the diagonal terms. All of the observed curvature of apparent resistivity and phase in the off-diagonal terms, and the finite values for the diagonal terms, are produced by 3-D seafloor topography. The topographic effect is most significant at the saddle between the two seamounts (site A), where divergence from 100 Ω m in the off-diagonal apparent resistivity is large and the diagonal apparent resistivity varies between 5 and 45 Ω m, more than one order of magnitude larger than is observed at sites B and C. This simple example illustrates the overwhelming importance of distortion on seafloor data.

[18] Applying any inversion method to MT responses distorted by seafloor topography can lead to an incorrect resistivity model for the mantle. To demonstrate this, we attempt to carry out 1-D inversion for the three distorted MT responses. First, we compute the square root of the determinant of the MT impedance tensor, Z_{det}, defined as

$$Z_{\mathrm{det}} = \sqrt{Z_{xx}Z_{yy} - Z_{xy}Z_{yx}}. \tag{13}$$

Z_{det} is invariant to rotation of a horizontal coordinate system and is frequently used to estimate the average 1-D structure. An alternative invariant, the Berdichevsky or arithmetic average of the off-diagonal terms [*Berdichevsky and Dmitriev*, 1976], will yield similar results. The Occam 1-D inversion method of *Constable et al.* [1987] is applied to the apparent resistivity and phase for Z_{det} with 3% noise free error (Figure 5a). The models for sites A–C are distinct and none of them is a half-space, as can easily be anticipated from the responses. A peak in conductivity appears at about 200 km, 50 km, and 100 km in the results for sites A, B, and C, respectively. This artificial feature could lead to structural misinterpretation.

[19] We now demonstrate the iterative topographic effect correction and 1-D inversion for mantle structure. We use the MT response at site A as the synthetic data set, $\mathbf{Z}_o$. Two cases are tested: (1) addition of 3% error without noise to the data and (2) addition of 3% error with 3% Gaussian noise. The apparent resistivities and phases for the synthetic $\mathbf{Z}_o$ are plotted in Figure 6. In these examples, we use 1-D models fit to the uncorrected MT response as the starting structure. The initial models are obtained by inverting Z_{det} calculated from each $\mathbf{Z}_o$. We simulate $\mathbf{Z}$ including topography using FS3D. $\mathbf{Z}_m$ is obtained from 1-D forward modeling because the 1-D algorithm is much faster than FS3D. The initial RMS misfits are 3.6 for the data without noise

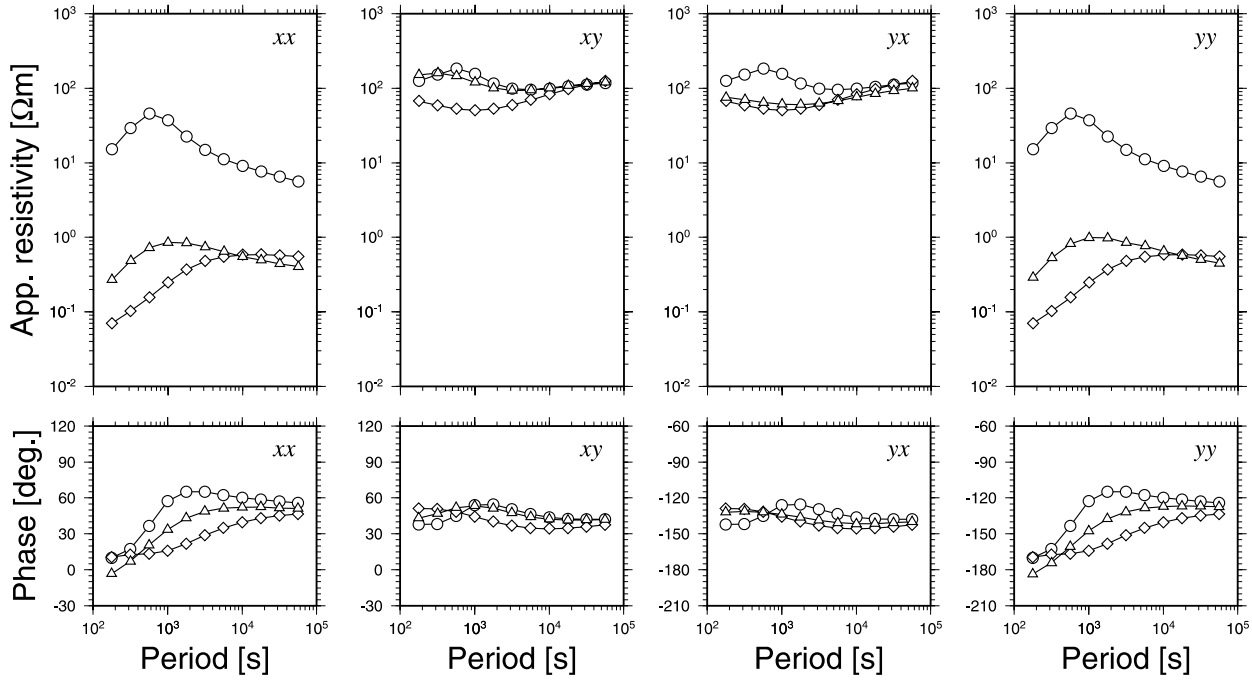

Figure 4. Synthetic tensor apparent resistivity and phase at the three locations shown in Figure 2. Circles, diamonds, and triangles are the responses for positions A, B, and C, respectively.

and 4.2 for the data with 3% Gaussian noise, respectively. The tests successfully recover the true structure after several iterations. The inversion results and RMS misfit at each stage are plotted in Figures 6, 7, and 8. The modeled conductivity become more constant with depth at successive iterations, and approaches the true structure of a 100 Ω m half-space. For the synthetic data without noise, the procedure converges after only one iteration. The MT response

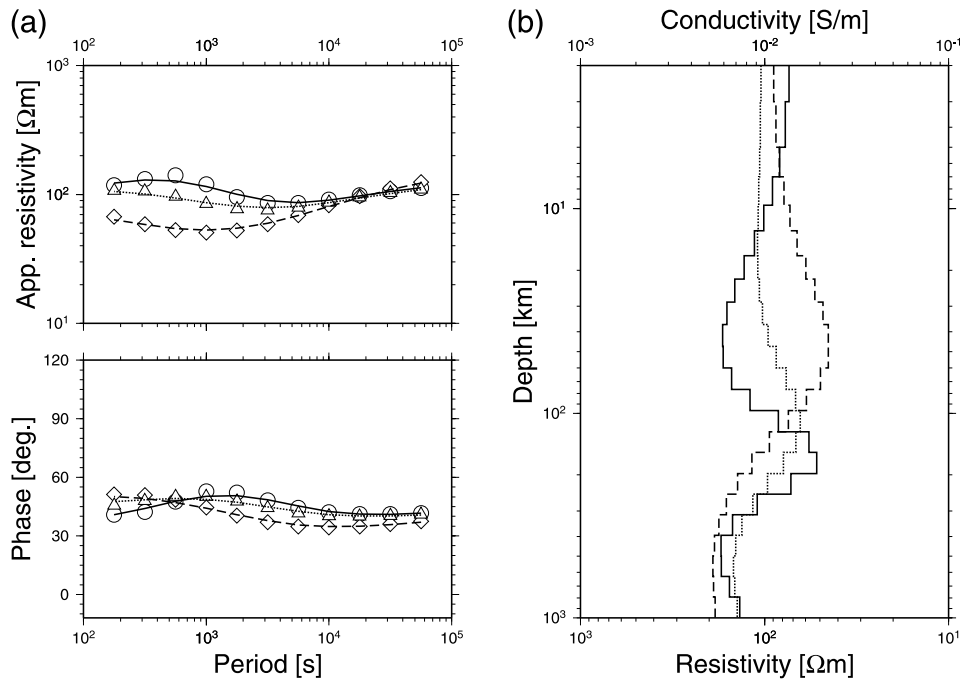

Figure 5. (a) Apparent resistivity and phase for the square root of the determinant of the MT impedance tensor (circles, diamonds, and triangles are for sites A, B, and C, respectively), along with the fit of a 1-D model to them (solid, dashed, and dotted lines, respectively). (b) The 1-D conductivity models obtained by Occam inversion of the determinant impedance tensor (solid, dashed, and dotted lines are for sites A, B, and C, respectively).

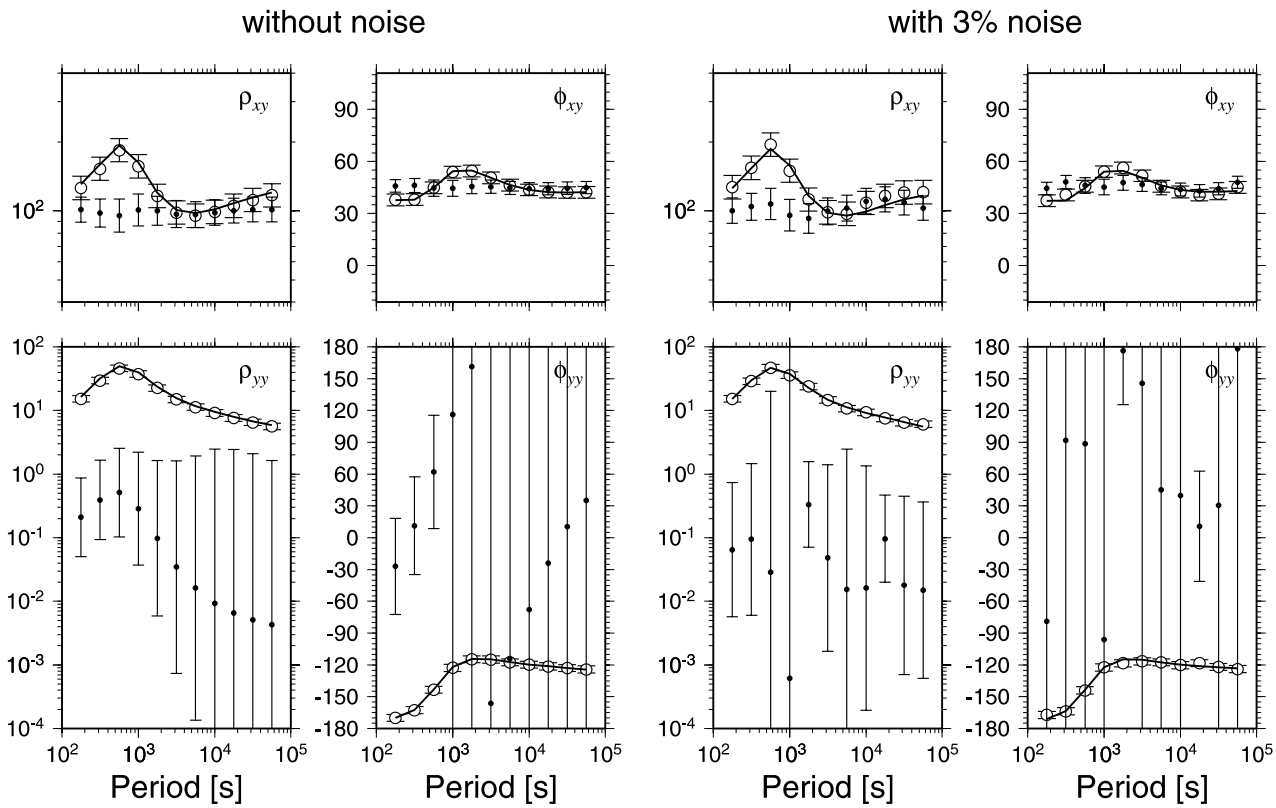

Figure 6. Apparent resistivities and phases used for the synthetic inversion test. (left) Data without noise and (right) data with 3% Gaussian noise. Only the *xy* and *yy* responses are plotted because the *yx* and *xx* responses are similar to the *xy* and *yy* responses, respectively. Open and solid circles are the original data and data corrected for the topographic effect at the final iteration stage, respectively. Solid lines are the model responses calculated from the final 1-D structures with topography.

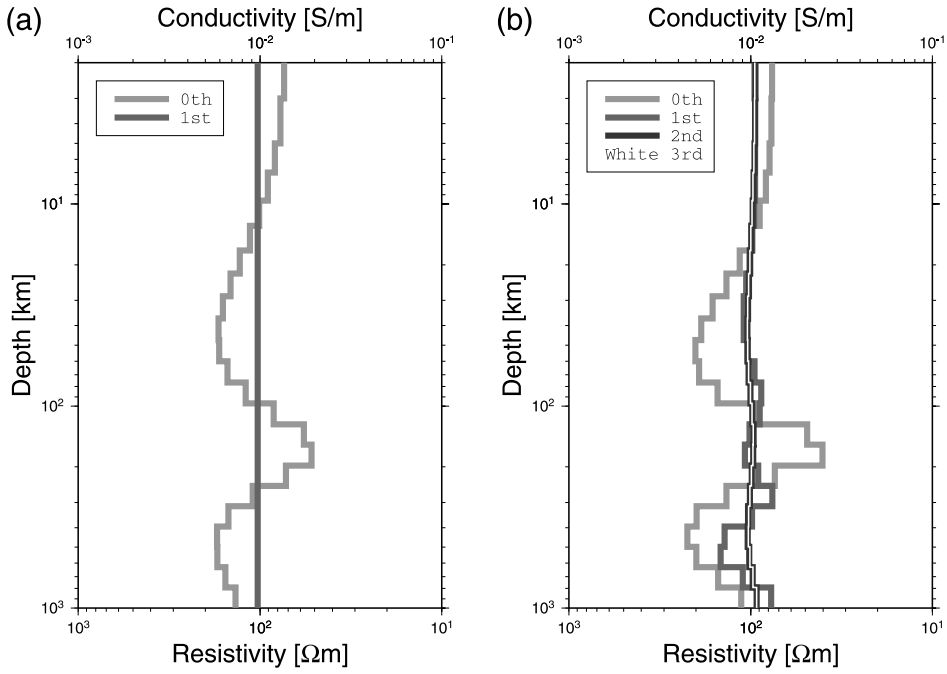

Figure 7. The 1-D conductivity models obtained by Occam inversion at each iteration stage. (a) For inversion of synthetic data without noise and (b) for inversion of synthetic data with 3% Gaussian noise. The models at the initial iteration are the models without topographic correction.

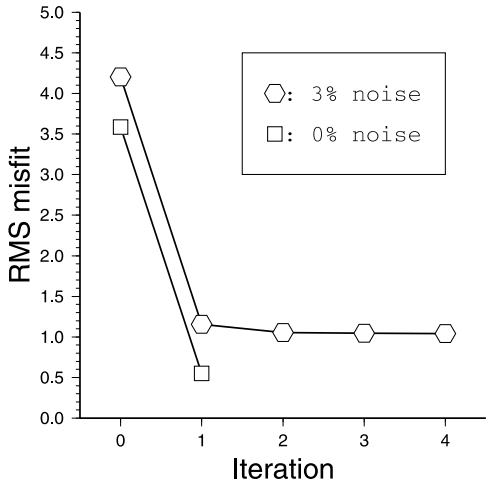

Figure 8. RMS misfit at each iteration stage.

corrected at the first iteration is already homogeneous with period in the *xy* and *yx* terms, and has negligible *xx* and *yy* terms (Figure 6). The final model is a half-space of 103 Ω m at a normalized RMS misfit of 0.6. The test for the synthetic data with 3% Gaussian noise converged at the third iteration. The corrected apparent resistivity and phase of the off-diagonal terms at this point are close to 100 Ω m and 45 or −135 degrees over the whole period range, although there are small variations due to noise (Figure 6). The resulting models change very little between the second and third iteration, and lie very close to the true half-space structure. The final normalized RMS misfit is 1.0, which is the expected value for data having independent, Gaussian-distributed errors. The tests for the synthetic data at sites B and C also showed similar results, although they are not plotted in the figures.

4. Mantle Electromagnetic and Tomography Experiment (MELT) Data Example

[20] The method is next applied to a seafloor MT data set from the Mantle ELectromagnetic and Tomography (MELT) experiment on the East Pacific Rise (EPR) at 17°S in 1996–1997. In this paper, we describe the topographic effects in the data and compare the corrected responses with those derived by [*Evans et al.*, 1999] using *Nolasco et al.*'s [1998] thin sheet method. The mantle structure obtained using the corrected data and its interpretation is described by *Baba et al.* [2005].

[21] Figure 9 shows a bathymetric map of the MELT region with the observation sites superimposed. There are two survey lines crossing the EPR spreading axis. We apply the topographic correction method to the data set from the denser southern line which crosses the ridge axis at a segment which is believed to be melt-rich based on topographic morphology. The full MT impedance tensor was

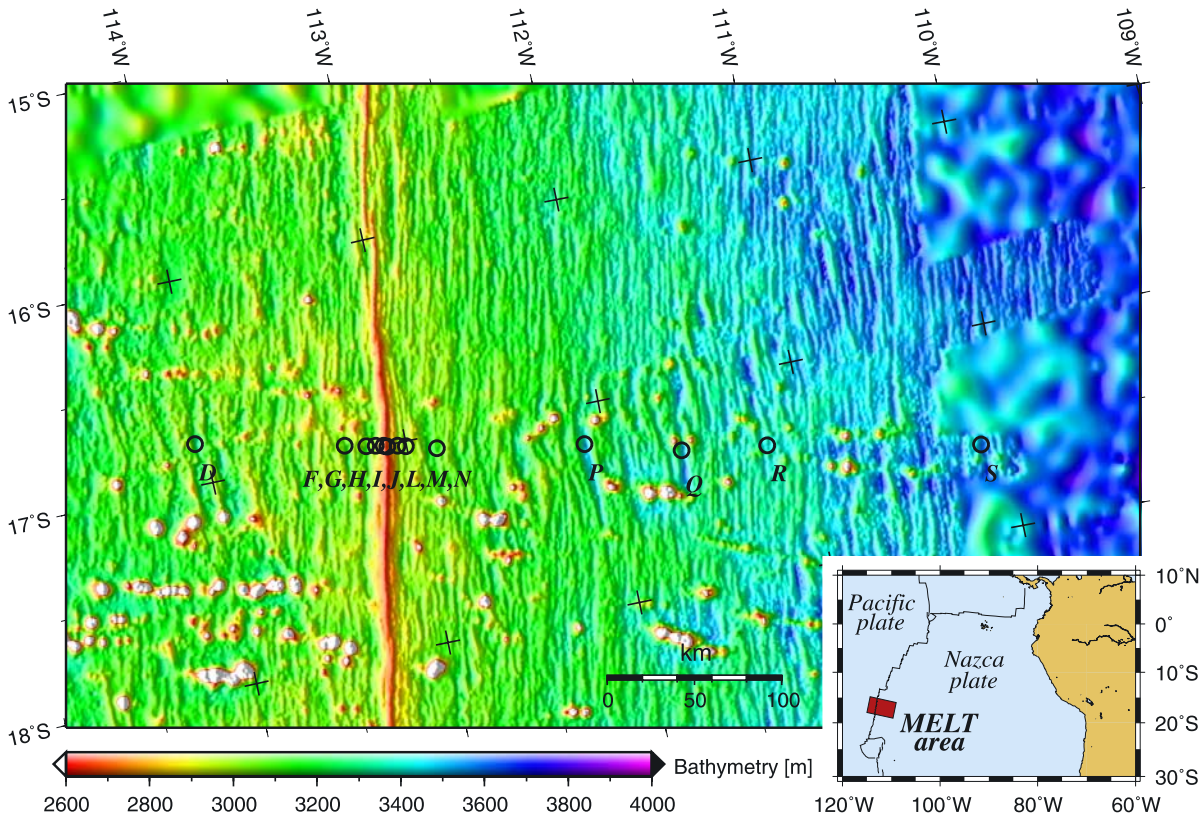

Figure 9. Bathymetric map of the MELT region. The map was created by combining multibeam data on a 1 km mesh [*Scheirer et al.*, 1998] with coarser predicted bathymetry (2' mesh) from *Smith and Sandwell* [1994]. The circles with labels are the sites where the MT responses were obtained.

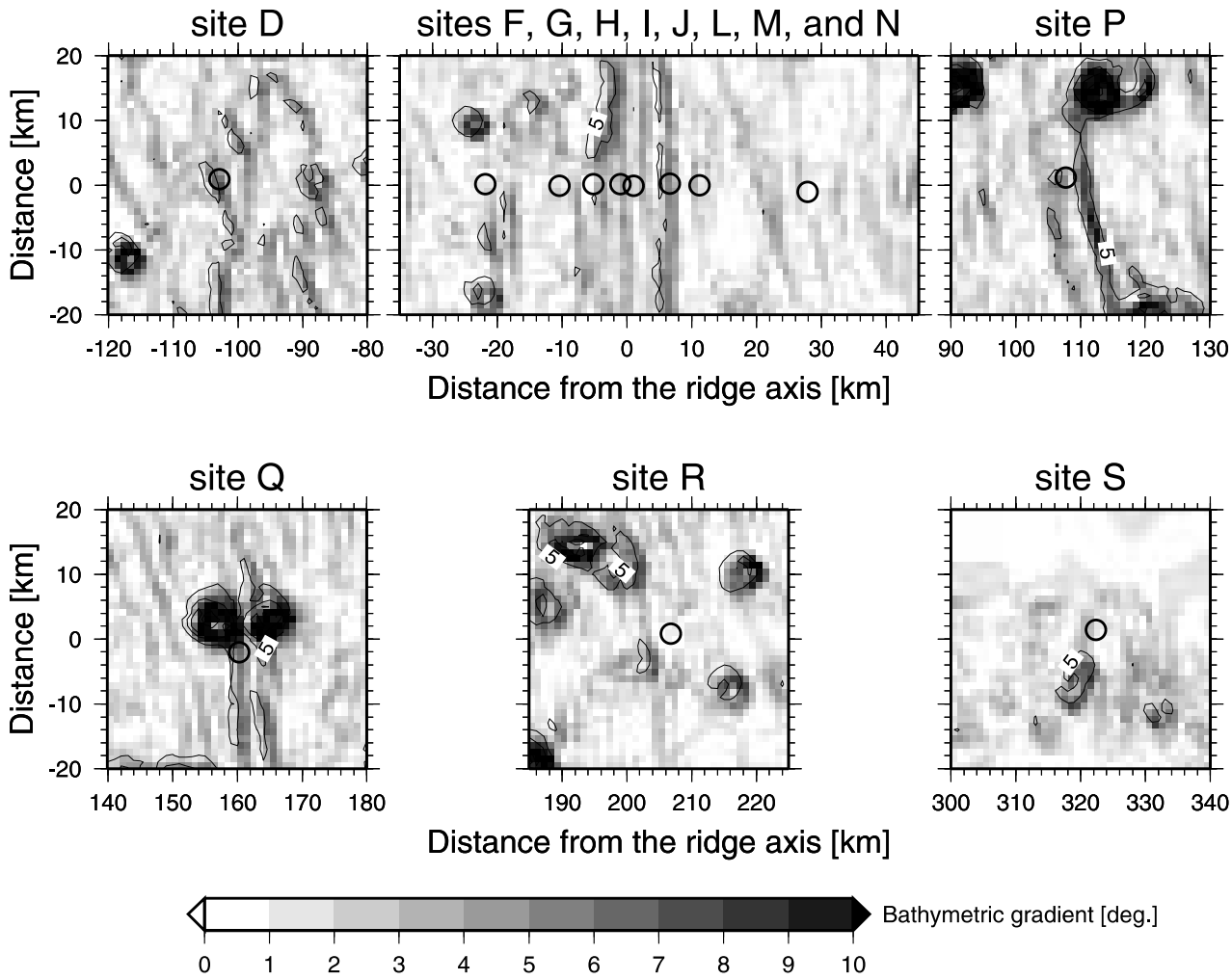

Figure 10. Gradient of bathymetry around observation sites. Circles indicate the site locations.

obtained at 13 sites using a bounded influence method [*Chave and Thomson*, 2003, 2004], as described by *Baba et al.* [2005].

[22] The topography in the MELT region is regionally two-dimensional and locally three-dimensional. The dominant feature of the topography is the EPR ridge crest and its thermal subsidence to either side. The ridge segment is quite linear and extends about 800 km from the Garrett Transform at ~13.5°S to the large overlapping spreading center (OSC) at 20°40s. On a finer scale, the segment is disrupted by a series of small discontinuities manifest as axial water depth variation. The southern survey line was located near the segment center where the ridge crest is shallowest (~2600 m, or ~300 m above the background seafloor) and widest (~20 km). The observed seafloor subsidence is asymmetric; the Pacific flank subsides at about half the rate of the Nazca flank [*Scheirer et al.*, 1998]. There are numerous linear topographic features subparallel to the ridge axis which are associated with faulting. Some lineaments are slightly oblique to the ridge axis because of crustal formation associated with the migration of OSCs [*Cormier et al.*, 1996]. There also are numerous off-axis seamounts, especially on the Pacific side.

[23] The seafloor topography model must be converted to a numerical mesh. We combined two bathymetric data sets which have different resolution: 1 km mesh data are based on multibeam swath data from *Scheirer et al.* [1998], and 2′ mesh bathymetric predictions from satellite altimetry and shipboard sounding data by *Smith and Sandwell* [1994] were used to fill gaps where multibeam data were not available. An area of 4032 × 4320 km centered on the southern survey line but rotated 12 degrees clockwise to align with the strike of the EPR axis was discretized for FS3D modeling, so that the x and y axes of the model are parallel and perpendicular to the EPR axis, respectively. The mesh resolution is finer (1–2 km) around the observation sites and coarser at more distant points in order to make the computation tractable. As a result, the number of grid cells is 37 in the along axis direction and 140 in the across axis direction, respectively. The vertical mesh is set so that there are 4 water layers and 42 layers below the seafloor down to about 1000 km depth. The change in bathymetry is flattened to a water depth of 3200 m and converted into changes in anisotropic conductivity and permeability in the lowermost seawater layer and the uppermost crustal layer, according to the FS3D algorithm. FS3D can simulate the topographic

Table 2. One-Dimensional Conductivity Model Used as the Initial Mantle Model for Topographic Effect Correction of the MELT MT Responses

Depth, km	Conductivity, S m^{-1}
0.00–3.20	3.2
3.20–9.39	0.001
9.39–51.49	0.0002
51.49–393.29	0.02
>393.29	1.0

response in the MELT area accurately because the gradient of the bathymetry around the observation sites are typically less than 5 degrees (Figure 10). However, there are two seamounts near site Q whose slope is close to 10 degrees. The seamounts may cause inaccurate modeling for the responses at site Q. We further discuss this issue later. The conductivity of seawater was set at 3.2 S m^{-1} and a 1-D layered model was used for an initial guess at the mantle structure as shown in Table 2. The initial model was formulated by approximating the 2-D model of *Evans et al.* [1999] into four layers, also taking account of typical oceanic lithosphere and asthenosphere features based on observations [e.g., *Heinson and Lilley*, 1993; *Lizarralde et al.*, 1995; *Nolasco et al.*, 1998].

[24] The MELT MT responses were obtained at various periods in the range from 250 to 92,160 s, depending on the sample rate for different instruments at different sites. The total number of periods is 30, which is too many to reasonably simulate. Since the MT response changes smoothly with period, we modeled the responses for seven periods equally sampled in log space, and interpolated the values for the intermediate periods using a natural spline.

[25] Figures 11 and 12 show pseudosections of the original and corrected apparent resistivity and phase. The observed MT responses are quasi-2-D in that the off-diagonal apparent resistivities are much larger than the diagonal terms. Other characteristic features are seen at sites located on the ridge crest. The along-strike *xy* apparent resistivity at the ridge crest is lower than that at distant sites, while the cross-strike *yx* apparent resistivity at the ridge crest is statically shifted higher. The *xy* phase is also smaller, especially at periods shorter than 4000 s. The region distant from the ridge crest displays relatively homogeneous features for both the apparent resistivity and phase.

[26] The topographic effect is evident when the responses before and after the correction are compared. Significant corrections are observed in the *xy* apparent resistivity and phase at the ridge crest and the off-diagonal phases at shorter periods at the easternmost four sites. The short-period *xy* phase at the ridge crest is increased by ~20 degrees, while the *xy* phase at the eastern sites, especially P and Q (~110 and ~160 km far from the ridge), decrease from ~110 to ~75 degrees at the shortest periods (see also Figure 13). The reverse sense of this change is due to local topography. The ridge crest sites are on topographic highs, while the off-ridge sites are typically located in valleys (Figure 9). A similar trend is predicted by the analytic study of *Schwalenberg and Edwards* [2004].

[27] The *yx* phases at the eastern sites are changed by the correction, but not by as much as the *xy* phases. The *yx* apparent resistivity is reduced nearly independent of period at most of the sites. The differences in the *yx* apparent resistivities before and after the correction are due to a galvanic charge effect for the approximately 2-D regional increase in water depth due to thermal subsidence. The diagonal terms of $\mathbf{Z}$ simulated by FS3D are typically so small that the *xx* and *yy* responses are corrected similarly to the *xy* and *yx* responses, respectively (Figure 13). This relation may be confirmed by ignoring the diagonal terms of $\mathbf{Z}$ in (11);

$$\mathbf{Z}_c \approx \begin{bmatrix} \frac{Z_{mxy}}{Z_{xy}} Z_{oxx} & \frac{Z_{mxy}}{Z_{xy}} Z_{oxy} \\ \frac{Z_{myx}}{Z_{yx}} Z_{oyx} & \frac{Z_{myx}}{Z_{yx}} Z_{oyy} \end{bmatrix} = \begin{bmatrix} \alpha Z_{oxx} & \alpha Z_{oxy} \\ \beta Z_{oyx} & \beta Z_{oyy} \end{bmatrix}, \quad (14)$$

where the diagonal terms of $\mathbf{Z}_m$ are zero because the mantle is 2-D. These results indicate that the topographic effect in the MELT area is dominantly 2-D.

[28] We compare the responses corrected for the topographic effect in this study with the thin sheet results from *Evans et al.* [1999]. Figure 13 compares these results with the observed responses at sites I and Q, located at the ridge axis and well off-axis, respectively. The corrected responses are very similar, suggesting that both methods work well for the most part. Small differences are seen in the diagonal terms at both sites. The cause of the difference is not clear because many parameters differ, such as the resolution of modeled topography and the assumed mantle structure in addition to the algorithm. The corrected response from *Evans et al.* [1999] is limited to periods longer than ~500 s (while the observed data exist down to 250 s) because the thin sheet approximation required by their forward modeling method breaks down at short periods. The responses corrected in this study do not suffer from such a limitation.

[29] The iterative process of topographic effect correction and inversion may be monitored through the normalized RMS misfit (Table 3). For the MELT data, a 2-D anisotropic inversion is applied [*Baba et al.*, 2005] with the sites on a flat 3200 m seafloor, and hence only the off-diagonal responses corrected for the topographic effect are inverted. The 2-D anisotropic model is incorporated into FS3D to obtain $\mathbf{Z}$, and then the misfit between $\mathbf{Z}$ and the observed response is assessed. $\mathbf{Z}_m$ is easily obtained from the forward responses from the 2-D anisotropic inversion. Both $\mathbf{Z}$ and $\mathbf{Z}_m$ are used for the correction at the next iteration. The misfits for the diagonal terms are much larger than those for the off-diagonal terms, and they don't improve with successive iterations because the 2-D model produces no diagonal response. This indicates that 3-D topographic effects are very small compared with 2-D effects, at least within the resolution of the model. Focusing on the misfit for the off-diagonal terms, the RMS misfit decreases significantly at the first iteration but is changed very little at the second iteration. Simultaneously, the essential features of the mantle conductivity model obtained from inversion also

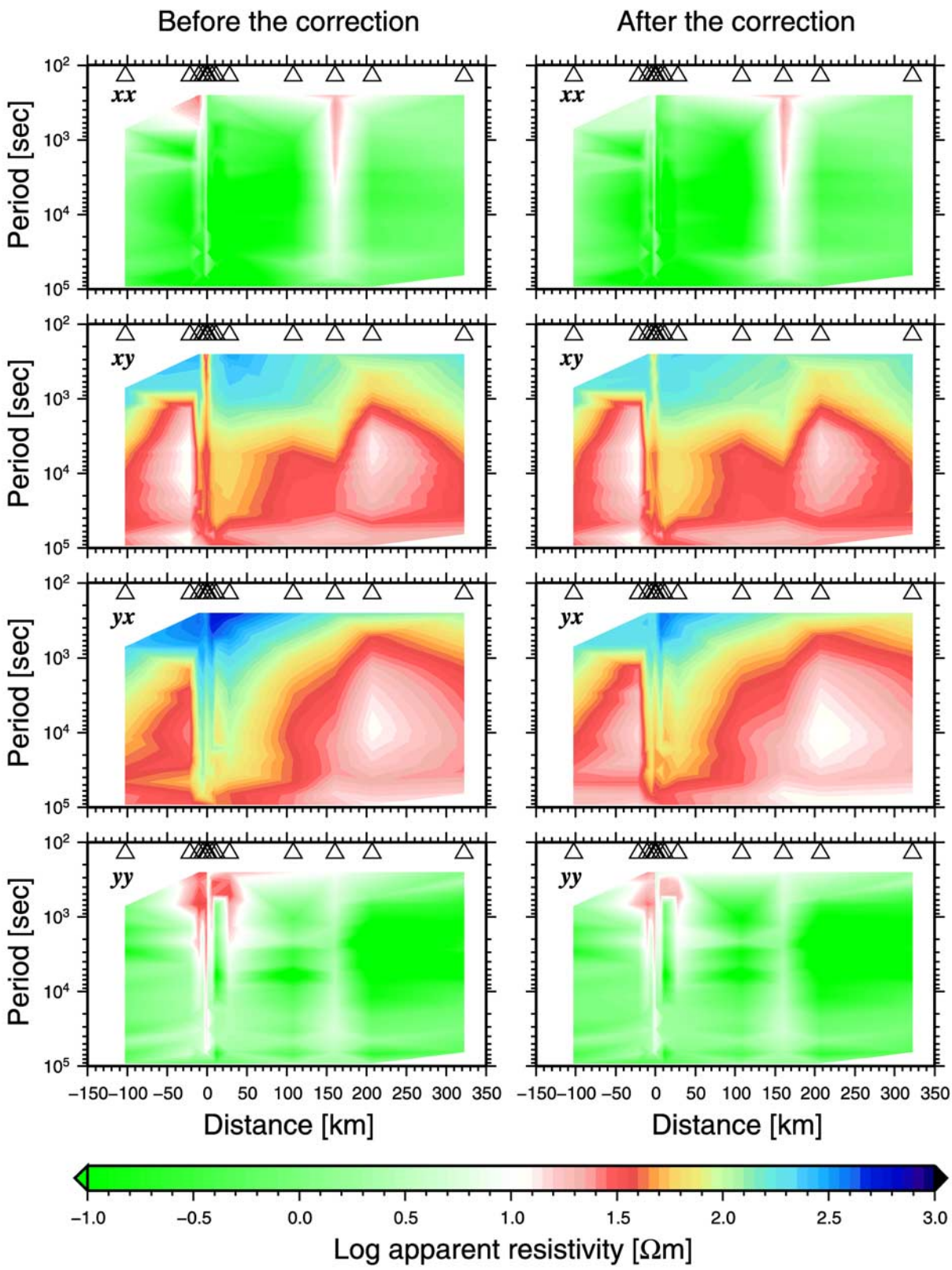

Figure 11. Pseudosection of apparent resistivities (left) before and (right) after the topographic correction. All terms of the tensor are plotted in rows. The horizontal axis is the distance from the ridge axis; *x* and *y* are the along- and across-ridge directions, respectively. Triangles indicate the location of the sites.

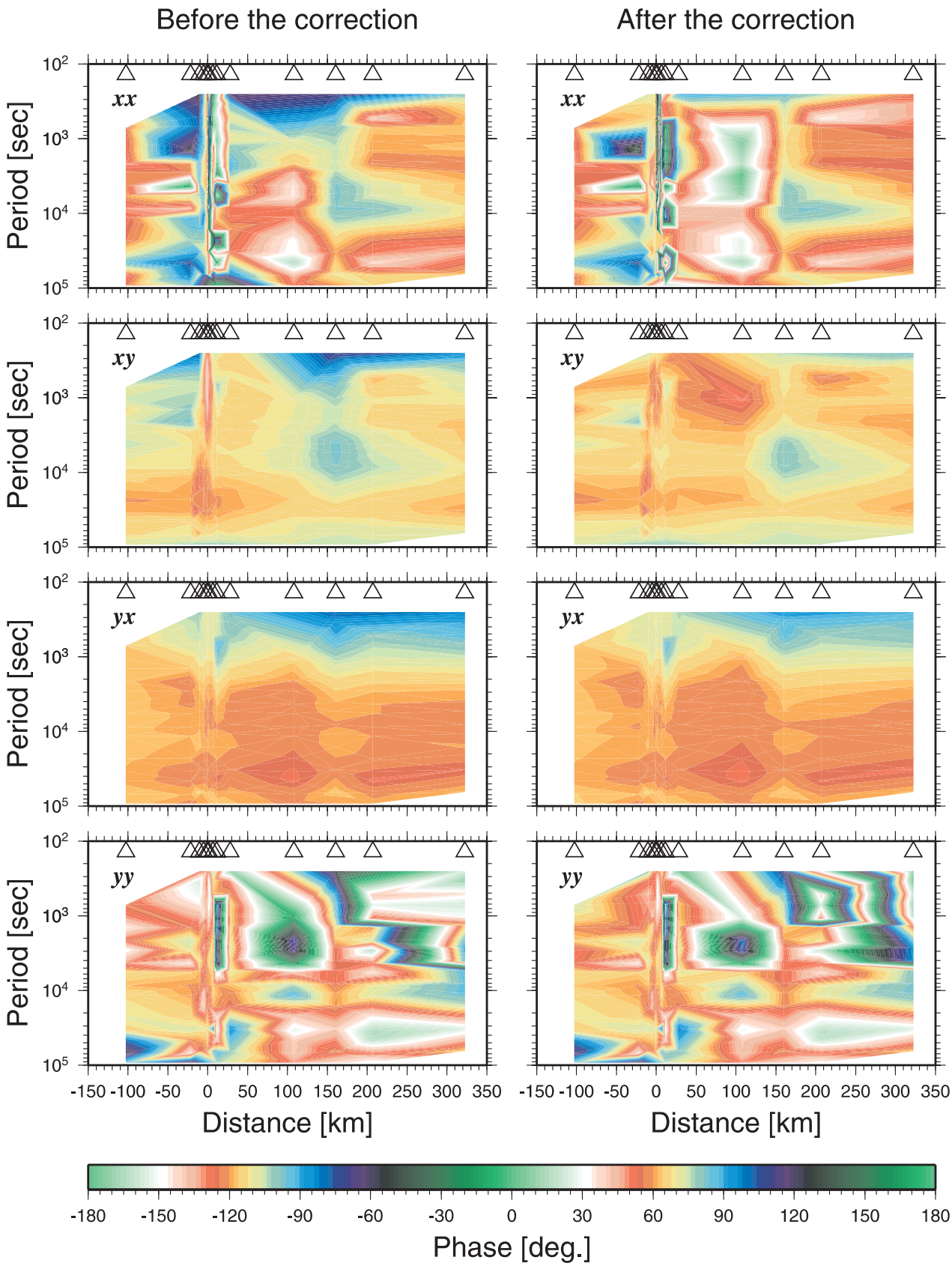

Figure 12. Pseudosections of phase (left) before and (right) after the topographic correction. See Figure 11 for details.

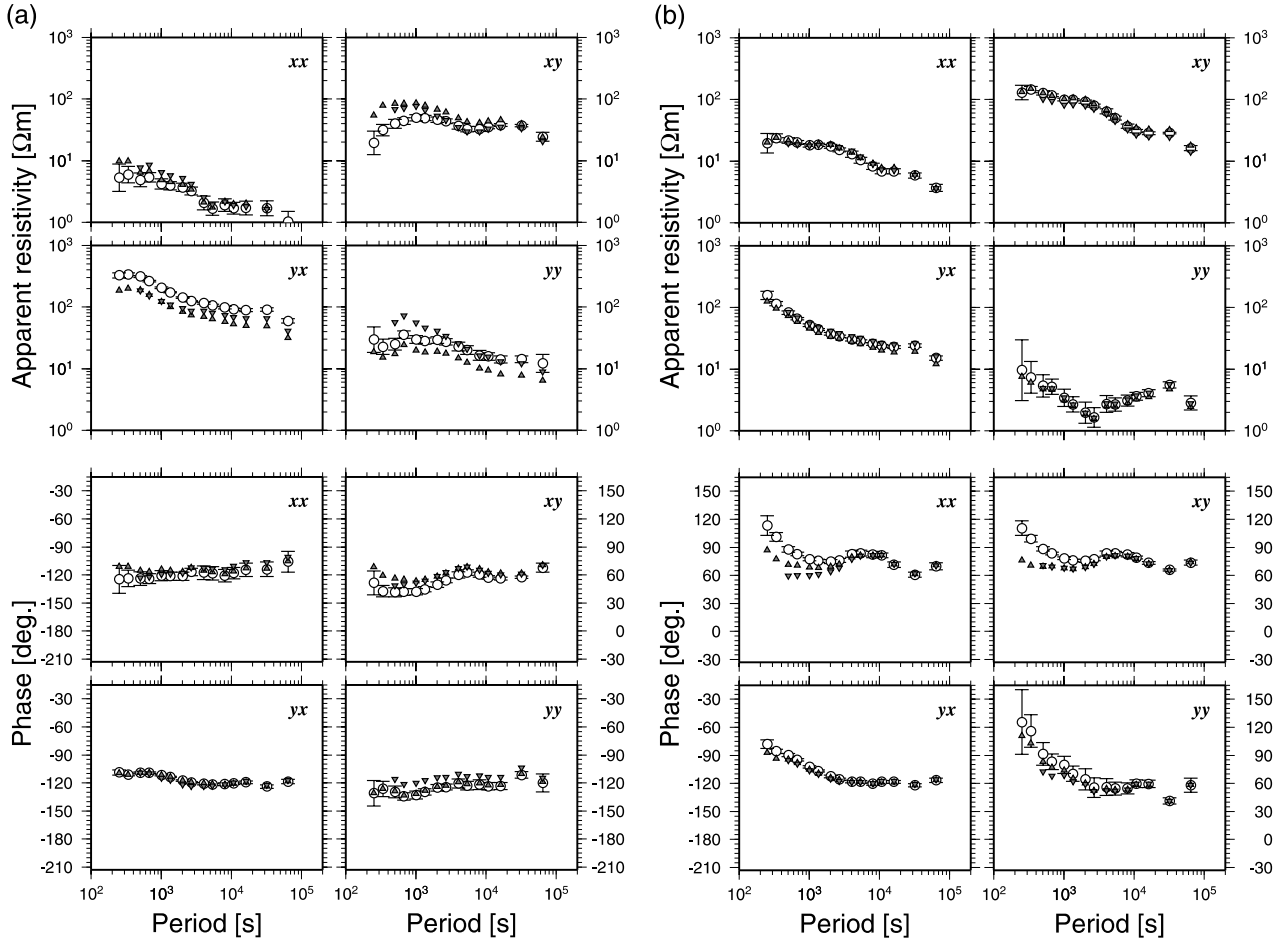

Figure 13. Apparent resistivities and phases for all terms of the MT impedance tensor at (a) site I (on the ridge crest) and (b) site Q (~160 km east of the ridge). Circles with error bars, triangles, and inverted triangles are the observed response, the response corrected for the topographic effect in this study, and the corrected response from *Evans et al.* [1999], respectively. The error bars for the corrected responses are omitted to show for clarity.

change very little, and the algorithm has converged. The RMS misfit of the *yx* term becomes slightly worse after the second iteration because of a poor fit to the apparent resistivity. A frequency-independent shift of the apparent resistivity (i.e., static shift) due to topographic effects is responsible. The cause of this static shift is discussed in section 5. The fit to the *yx* phase is good at all periods, as is that for all of the *xy* terms. Figure 14 shows the RMS misfit for the off-diagonal apparent resistivity and phase at each site. The misfits for the response except for the *yx* apparent resistivity are not significantly different for the first and second iterations.

5. Discussion

[30] We can provide a physical interpretation of $\mathbf{Z}_t$ in (9)–(11) for a situation where the following two assumptions hold: (1) the inductive scale of the mantle conductivity distribution is much larger than that of the topography and (2) the topographic change is such that the vertical electric field is small compared to the horizontal electric field. In this situation, $\mathbf{Z}_t$ can be related to complex electric and magnetic distortion tensors.

[31] From integral equation treatments of electromagnetic scattering by 3-D bodies [e.g., *Wannamaker et al.*, 1984; *Groom and Bahr*, 1992; *Chave and Smith*, 1994; *Nolasco et al.*, 1998], the relation between the MT impedance and distortion tensors is

$$\mathbf{E}(\mathbf{r}) = \mathbf{E}_m(\mathbf{r}) + i\omega\mu_0 \int_V \mathrm{g}(\mathbf{r},\mathbf{r}')\delta\sigma(\mathbf{r}')\mathbf{E}(\mathbf{r}')d\mathbf{r}' + \nabla\frac{1}{\sigma_m}\nabla\int_V \mathrm{g}(\mathbf{r},\mathbf{r}')\delta\sigma(\mathbf{r}')\mathbf{E}(\mathbf{r}')d\mathbf{r}' \quad (15)$$

$$\mathbf{B}(\mathbf{r}) = \mathbf{B}_m(\mathbf{r}) + \mu_0\nabla\times\int_V \mathrm{g}(\mathbf{r},\mathbf{r}')\delta\sigma(\mathbf{r}')\mathbf{E}(\mathbf{r}')d\mathbf{r}', \quad (16)$$

where σ_m refers to the mantle conductivity structure, $\mathbf{E}_m$ and $\mathbf{B}_m$ are the electromagnetic fields due to the regional mantle structure, $\delta\sigma(\mathbf{r}')$ is the conductivity heterogeneity due to topographic change, and $\mathrm{g}(\mathbf{r}, \mathbf{r}')$ is the appropriate scalar Green function. The second and third terms in (15) are the inductive and galvanic scattered components due to conductive inhomogeneity.

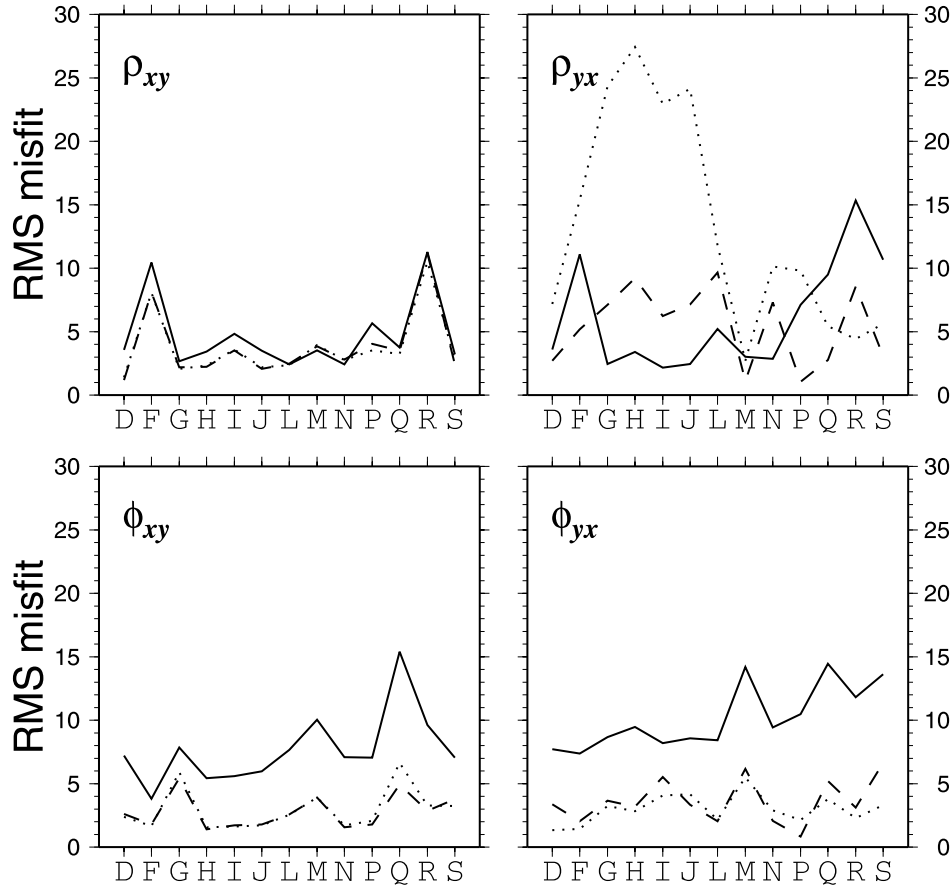

Figure 14. RMS misfit between the observed and calculated responses of the *xy* and *yx* terms at each site. Solid, dashed, and dotted lines are the misfit for the zeroth, first, and second iteration, respectively.

[32] Under the first assumption, these integral equations may be expressed in tensor form as

$$\mathbf{E}(\mathbf{r}) = \mathbf{C}\mathbf{E}_m(\mathbf{r}) \tag{17}$$

$$\mathbf{B}(\mathbf{r}) = \mathbf{B}_m(\mathbf{r}) + \mathbf{D}\mathbf{E}_m(\mathbf{r}), \tag{18}$$

where $\mathbf{C}$ and $\mathbf{D}$ are 3×3 complex electric and magnetic distortion tensors, respectively. If the second assumption is valid, (17) and (18) can be reduced to a relation between the horizontal fields so that $\mathbf{C}$ and $\mathbf{D}$ become 2×2 tensors. For galvanic distortion decomposition, these are further reduced to real tensors [*Groom and Bahr*, 1992; *Chave and Smith*, 1994] under the additional assumption that the inductive component is small compared with the galvanic component.

[33] The relation between the MT impedance and the observed horizontal electromagnetic field is written as $\mathbf{E} = \mathbf{Z}\mathbf{B}$ and, in the same way, $\mathbf{E}_m = \mathbf{Z}_m\mathbf{B}_m$ holds for the fields due to mantle structure. Combining these definitions with (17) and (18) gives

$$\mathbf{Z} = \mathbf{C}(\mathbf{I} + \mathbf{Z}_m\mathbf{D})^{-1}\mathbf{Z}_m, \tag{19}$$

where $\mathbf{I}$ is a 2×2 identity tensor, so that $\mathbf{Z}_t$ is expressed by

$$\mathbf{Z}_t = \mathbf{C}(\mathbf{I} + \mathbf{Z}_m\mathbf{D})^{-1}. \tag{20}$$

$\mathbf{Z}_t$ is a combination of the electric and magnetic field distortion tensors and the mantle response. The correction method of *Nolasco et al.* [1998] follows from similar considerations. They determine tensors corresponding to $\mathbf{C}$ and $\mathbf{D}$ by the numerical simulation of $\mathbf{E}$, $\mathbf{B}$, and $\mathbf{E}_m$, and then recover $\mathbf{Z}_m$ from the observed response using a rearrangement of (19). Consequently, the relevant physics for *Nolasco et al.* [1998] and in this study is identical, although its simulation is not.

[34] In the application of the topographic correction method to the MELT data, although most of the features of the corrected responses are similar to the results from the thin sheet modeling of *Evans et al.* [1999], there are small but significant differences between the corrected responses. As previously mentioned, with FS3D, the terms for each row of the observed tensors are corrected similarly at sites I and Q, so that the topographic effect is dominantly 2-D from (14). However, for the *Evans et al.* [1999] correction,

Table 3. RMS Misfit Between Observed ($\mathbf{Z}_o$) and Calculated ($\mathbf{Z}$) MT Responses at Each Iteration Stage

	RMS Misfits				
Iteration Stage	*xx*	*xy*	*yx*	*yy*	Total
Zeroth	34.030	6.960	9.074	44.365	28.535
First	32.066	3.949	5.244	47.065	28.664
Second	38.475	3.985	11.137	50.019	32.102

the resultant *yy* apparent resistivity at site I is shifted upward, which is opposite in sense to the corrected *yx* apparent resistivity. Further, the *yy* phase is shifted independently of period while the *yx* phase changes very little. Such differences are not obvious at site Q. The results from FS3D indicate that topographic influence is dominantly 2-D at both sites I and Q, while the results from *Evans et al.* [1999] indicate that 3-D effects make some contribution at site I but little at site Q. Figures 9 and 10 show a very 2-D ridge crest around site I and some 3-D features due to the presence of a pair of seamounts near site Q. The sense of the correction of *Evans et al.* [1999] is qualitatively inconsistent with the observed topographic features. However, the limited effect of the 3-D features near site Q for FS3D may also be suspect, and may reflect the resolution of the bathymetry available for modeling. We attempted to check the impact of the mesh design for FS3D by using a finer mesh around site Q, with an indecisive outcome. The real data may be affected by unresolved small-scale local topography. No modeling method can determine the effect of features that are unresolved in the bathymetric data. In addition, the accuracy of FS3D may be reduced around the seamounts near site Q. As shown in section 2, the FS3D responses are accurate for topography with a slope below $\sim$5 degrees. However, the two seamounts near site Q have gradient close to 10 degrees.

[35] The topographic effect correction and inversion algorithm applied to the MELT data converged after only two iterations, although the RMS misfit of the *yx* apparent resistivity increased during the last iteration. This indicates that the topographic effect in the MELT area is reasonably robust to assumptions about the subsurface structure. A weak dependence of the distortion matrices (**C** and **D**) on the mantle structure was also seen in the Society islands area [*Nolasco et al.*, 1998]. The misfit of the *yx* apparent resistivity is probably due to heterogeneous conductivity immediately beneath the seafloor introduced during 2-D inversion. Such heterogeneities can result in large changes in the apparent topographic effect, especially in a galvanic sense, compared to the effect for the initial 1-D mantle structure. In fact, under the conditions where (20) holds, it is evident that $\mathbf{Z}_t$ is dependent on $\mathbf{Z}_m$ as well as **C** and **D**, and $\mathbf{Z}_m$ contains the effect of near-surface heterogeneities in practical calculations. Since the observed data are not sensitive to such near-surface structure, the heterogeneities and resultant change in topographic effects are thought to be artificial. For application of the iterative method to 2-D or 3-D mantle structure in future studies, and in order to stabilize its convergence, the inversion should be carried out with a strategy that prevents near surface heterogeneity from being introduced.

6. Conclusions

[36] We describe an iterative method for seafloor MT data analysis that is a combination of precise topographic effect correction and subsequent inversion of topographically stripped data for mantle structure. The topographic effect is defined as a tensor multiplying the MT impedance tensor associated with mantle structure, and is removed from the observed MT response. Adopting FS3D by *Baba and Seama* [2002] for forward modeling of topography allows us to model topographic change over an arbitrary mantle structure without the thin sheet approximation, and to check the mutual coupling between the topographic effect and deep mantle structure by iteration of the topographic correction and inversion.

[37] The method has been applied to synthetic and real data. Tests for synthetic data from 3-D topography over a half-space show that the method works well in cases where the data do and do not contain noise. From application to real seafloor MT data collected in the MELT experiment, we obtained similar corrected responses to those by *Evans et al.* [1999] from thin sheet modeling. However, the responses corrected in this study extend to shorter periods than *Evans et al.*'s [1999] responses because the present algorithm does not suffer from the inherent limitation of the thin sheet approximation. The iterative method converged successfully except for the *yx* apparent resistivity, probably due to the effect of poorly resolved near-surface heterogeneities produced during inversion.

[38] **Acknowledgments.** We thank Daniel S. Scheirer for providing the digital bathymetry data in the MELT region and Rob L. Evans and Pascal Tarits for the MT responses observed and corrected for the topographic effect used by *Evans et al.* [1999]. Katrin Schwalenberg provided a computer program for calculating analytical solutions to synthetic topography models. Rob L. Evans and Nobukazu Seama gave us helpful comments on the draft. All figures were produced using GMT software [*Wessel and Smith*, 1998]. This work was supported by NSF grants OCE9402324 and OCE0118254 and Research Program on Mantle Core Dynamics, Institute for Research on Earth Evolution (IFREE), Japan Agency for Marine-Earth Science and Technology (JAMSTEC).

References

Baba, K., and N. Seama (2002), A new technique for the incorporation of seafloor topography in electromagnetic modeling, *Geophys. J. Int.*, *150*, 392–402.

Baba, K., A. D. Chave, R. L. Evans, G. Hirth, and R. L. Mackie (2005), Mantle dynamics beneath the East Pacific Rise at 17°S: Insights from the MELT EM data, *J. Geophys. Res.*, doi:10.1029/2004JB003598, in press.

Bahr, K. (1988), Interpretation of the magnetotelluric impedance tensor: Regional induction and local telluric distortion, *J. Geophys.*, *62*, 119–127.

Berdichevsky, M. N., and V. I. Dmitriev (1976), Distortion of magnetic and electric fields by near-surface lateral inhomogeneities, *Acta Geod. Geophys. Montanist. Acad. Sci. Hung.*, *11*, 447–483.

Berdichevsky, M. N., L. L. Vanyan, and V. I. Dmitriev (1989), Methods used in the U.S.S.R. to reduce near-surface inhomogeneity effects on deep magnetotelluric sounding, *Phys. Earth Planet. Inter.*, *53*, 194–206.

Chave, A. D., and J. T. Smith (1994), On electric and magnetic galvanic distortion tensor decompositions, *J. Geophys. Res.*, *99*, 4669–4682.

Chave, A. D., and D. J. Thomson (2003), A bounded influence regression estimator based on the statistics of the hat matrix, *J. Roy. Stat. Soc., Series C, (Appl. Stat.)*, *52*, 307–322.

Chave, A. D., and D. J. Thomson (2004), Bounded influence estimation of magnetotelluric response functions, *Geophys. J. Int.*, *157*, 988–1006, doi:10.1111/j.1365-246X.2004.02203.x.

Constable, S. C., R. L. Parker, and C. G. Constable (1987), Occam's inversion: A practical algorithm for generating smooth models from electromagnetic sounding data, *Geophysics*, *52*(3), 289–300.

Cormier, M. H., D. S. Scheirer, and K. C. Macdonald (1996), Evolution of the East Pacific Rise at 16°–19°S since 5 Ma: Bisection of overlapping spreading centers by new, rapidly propagating ridge segments, *Mar. Geophys. Res.*, *18*, 53–84.

Evans, R. L., et al. (1999), Asymmetric electrical structure in the mantle beneath the East Pacific Rise at 17°S, *Science*, *286*, 752–756.

Filloux, J. H. (1977), Ocean-floor magnetotelluric sounding over North Central Pacific, *Nature*, *262*, 297–301.

Groom, R. W., and K. Bahr (1992), Corrections for near surface effects: Decomposition of the magnetotelluric impedance tensor and scaling corrections for regional resistivities: A tutorial, *Surv. Geophys.*, *13*, 341–379.

Groom, R. W., and R. C. Bailey (1989), Decomposition of magnetotelluric impedance tensors in the presence of local three-dimensional galvanic distortion, *J. Geophys. Res.*, *94*, 1913–1925.

Heinson, G., and F. E. M. Lilley (1993), An application of thin-sheet electromagnetic modelling to the Tasman Sea, *Phys. Earth Planet. Inter.*, *81*, 231–251.

Jiracek, J. G. (1990), Near-surface and topographic distortions in electromagnetic induction, *Surv. Geophys.*, *11*, 163–203.

Koyama, T. (2002), A study of the electrical conductivity of the mantle by voltage measurements for submarine cables, Ph.D. thesis, Univ. Tokyo, Tokyo.

Lizarralde, D., A. Chave, G. Hirth, and A. Schultz (1995), Northeastern Pacific mantle conductivity profile from long-period magnetotelluric sounding using Hawaii-to-California submarine cable data, *J. Geophys. Res.*, *100*, 17,837–17,854.

Mackie, R. L., J. T. Smith, and T. R. Madden (1994), Three-dimensional electromagnetic modeling using finite difference equation: The magnetotelluric example, *Radio Sci.*, *29*(4), 923–935.

Nolasco, R., P. Tarits, J. H. Filloux, and A. D. Chave (1998), Magnetotelluric imaging of the Society Islands hotspot, *J. Geophys. Res.*, *103*, 30,287–30,309.

Oldenburg, D. W., K. P. Whittall, and R. L. Parker (1984), Inversion of ocean bottom magnetotelluric data revisited, *J. Geophys. Res.*, *89*, 1289–1833.

Scheirer, D. S., D. W. Forsyth, M. H. Cormier, and K. C. Macdonald (1998), Shipboard geophysical indications of asymmetry and melt production beneath the East Pacific Rise near the MELT experiment, *Science*, *280*, 1221–1224.

Schwalenberg, K., and R. N. Edwards (2004), The effect of seafloor topography on magnetotelluric fields: An analytical formulation confirmed with numerical results, *Geophys. J. Int.*, *159*, 607–621, doi:10.1111/j.1365-246X.2004.02280.x.

Smith, W. H., and D. T. Sandwell (1994), Bathymetric prediction from dense altimetry and sparse shipboard bathymetry, *J. Geophys. Res.*, *99*, 21,803–21,824.

Utada, H., and H. Munekane (2000), On galvanic distortion of regional three-dimensional magnetotelluric impedances, *Geophys. J. Int.*, *140*, 385–398.

Vasseur, G., and P. Weidelt (1977), Bimodal electromagnetic induction in non-uniform thin sheets with an application to the northern Pyrenean induction anomaly, *Geophys. J. R. Astron. Soc.*, *51*, 669–690.

Wannamaker, P. E., G. W. Hohmann, and S. H. Ward (1984), Magnetotelluric responses of three-dimensional bodies in layered earths, *Geophysics*, *49*(9), 1517–1533.

Wannamaker, P. E., J. R. Booker, A. G. Jones, A. D. Chave, J. H. Filloux, H. S. Waff, and L. K. Law (1989), Resistivity cross section through the Juan de Fuca subduction system and its tectonic implications, *J. Geophys. Res.*, *94*, 14,127–14,144.

Wessel, P., and W. H. F. Smith (1998), New, improved version of the Generic Mapping Tools released, *Eos Trans. AGU*, *79*, 579.

White, S. N., A. D. Chave, and J. H. Filloux (1997), A look at galvanic distortion in the Tasman Sea and the Juan de Fuca plate, *J. Geomagn. Geoelectr.*, *49*(11,12), 1373–1386.

K. Baba, Earthquake Research Institute, University of Tokyo, 1-1-1, Yayoi, Bunkyo-ku, Tokyo, 113-0032, Japan. (kbaba@eri.u-tokyo.ac.jp)

A. D. Chave, Department of Applied Ocean Physics and Engineering, Woods Hole Oceanographic Institution, Woods Hole, MA 02543, USA. (alan@whoi.edu)